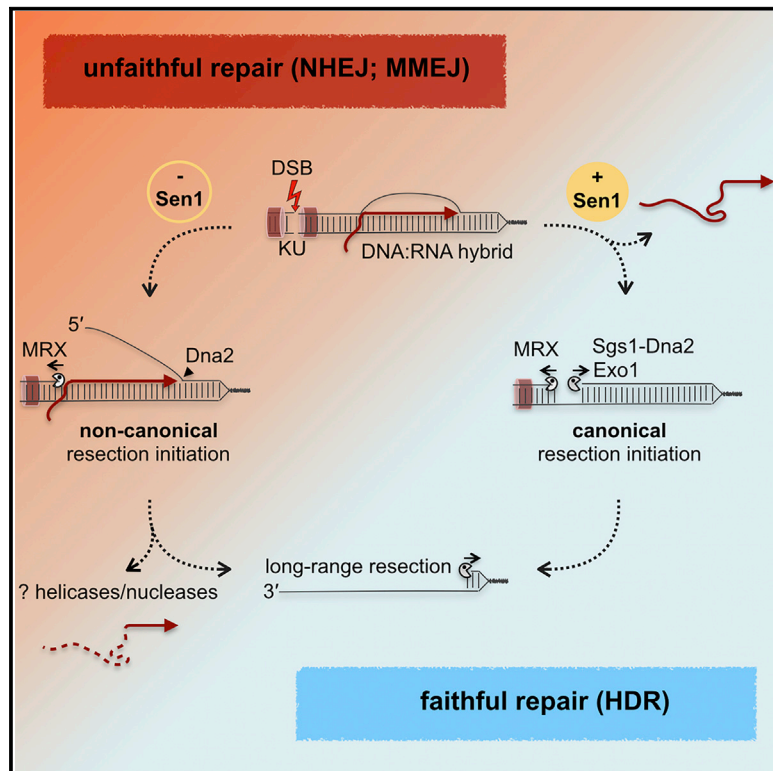# Senataxin Ortholog Sen1 Limits DNA:RNA Hybrid Accumulation at DNA Double-Strand Breaks to Control End Resection and Repair Fidelity

Graphical Abstract

Highlights

- Sen1 is recruited to DSBs in a Mre11-dependent manner

- DNA:RNA hybrids and repair factor KU persist at DSBs in the absence of Sen1

- DNA:RNA hybrids drive Mre11-Dna2-dependent non-canonical DSB resection initiation

- Non-canonical DSB resection initiation causes elevated NHEJ and translocations

Authors

Chetan C. Rawal, Luca Zardoni, Matteo Di Terlizzi, ..., Federico Lazzaro, Giordano Liberi, Achille Pellicioli

Correspondence

giordano.liberi@igm.cnr.it (G.L.), achille.pellicioli@unimi.it (A.P.)

In Brief

Rawal et al. identify a non-canonical mechanism of DSB processing in yeast cells lacking the Senataxin ortholog Sen1 helicase, which strictly depends on DNA:RNA hybrid formation at the break and is associated with unfaithful DSB repair and genome instability.

CellPress

Cell Reports

Article

Senataxin Ortholog Sen1 Limits DNA:RNA Hybrid Accumulation at DNA Double-Strand Breaks to Control End Resection and Repair Fidelity

Chetan C. Rawal,[1,5] Luca Zardoni,[2,3] Matteo Di Terlizzi,[1] Elena Galati,[1] Alessandra Brambati,[2,6] Federico Lazzaro,[1] Giordano Liberi,[2,4,*] and Achille Pellicioli[1,7,*]

[1]Dipartimento di Bioscienze, Università degli studi di Milano, 20131 Milan, Italy
[2]Istituto di Genetica Molecolare Luigi Luca Cavalli-Sforza, CNR, 27100 Pavia, Italy
[3]Scuola Universitaria Superiore IUSS, 27100 Pavia, Italy
[4]IFOM Foundation, 20139 Milan, Italy
[5]Present address: Molecular and Computational Biology Department, University of Southern California, Los Angeles, CA 90089, USA
[6]Present address: Skirball Institute of Biomolecular Medicine, Department of Cell Biology, NYU School of Medicine, New York, NY 10016, USA
[7]Lead Contact
*Correspondence: giordano.liberi@igm.cnr.it (G.L.), achille.pellicioli@unimi.it (A.P.)
https://doi.org/10.1016/j.celrep.2020.107603

SUMMARY

An important but still enigmatic function of DNA:RNA hybrids is their role in DNA double-strand break (DSB) repair. Here, we show that Sen1, the budding yeast ortholog of the human helicase Senataxin, is recruited at an HO endonuclease-induced DSB and limits the local accumulation of DNA:RNA hybrids. In the absence of Sen1, hybrid accumulation proximal to the DSB promotes increased binding of the Ku70-80 (KU) complex at the break site, mutagenic non-homologous end joining (NHEJ), micro-homology-mediated end joining (MMEJ), and chromosome translocations. We also show that homology-directed recombination (HDR) by gene conversion is mostly proficient in *sen1* mutants after single DSB. However, in the absence of Sen1, DNA:RNA hybrids, Mre11, and Dna2 initiate resection through a non-canonical mechanism. We propose that this resection mechanism through local DNA:RNA hybrids acts as a backup to prime HDR when canonical pathways are altered, but at the expense of genome integrity.

INTRODUCTION

Double-strand breaks (DSBs) are among the most deleterious types of lesion for the cell, whose improper repair can lead to inheritable genetic rearrangements, including gross chromosomal rearrangements. The regulation of the nucleolytic processing of the DSB ends (also called DSB resection) is critical in determining break repair through non-homologous end joining (NHEJ) or homology-directed recombination (HDR) (Symington, 2016). In preparation for HDR, DBS ends are nucleolytically resected to form 3′ single-stranded DNA (ssDNA) for the invasion of the homologous template, whereas NHEJ repair results in re-ligation of the DSB ends with minimal processing. Moreover, extended DNA end processing and annealing between micro-homologies primes DSB repair through micro-homology-mediated end joining (MMEJ) and single-strand annealing (SSA) (Seol et al., 2018). DSB resection is antagonized by the Ku70-80 (KU) complex, which rapidly binds to DNA ends and acts as a scaffold for other proteins involved in NHEJ (Frit et al., 2019). However, the Mre11-Rad50-Xrs2 complex (MRX; MRN in human), aided by the associated factor Sae2 (CtIP in human), overcomes the KU barrier, creating a nick close to the break and triggering DSB resection (Marini et al., 2019). Starting from the nick,

the exonuclease activity of MRX resects the DNA filament toward the DSB (a processed called short-range resection), while Exo1 and Dna2, in cooperation with the DNA helicase Sgs1 (BLM in human), process the DNA filament in the other direction (long-range resection) (Symington, 2016). This bidirectional mechanism leads to the formation of 3′ ssDNA, which is immediately covered by replication protein A (RPA) complex and later by the recombinase Rad51, promoting HDR.

Co-transcriptional DNA:RNA hybrids, which together with the displaced non-template DNA strand form R-loops, have been recently implicated in DSB repair (Jimeno et al., 2019; Puget et al., 2019). These structures are detected at both intergenic and intragenic DNA regions experiencing a DSB, raising the possibility that hybrids can be generated at broken ends by both pre-existing and *de novo* transcription. DNA:RNA hybrids/R-loops were shown to promote HDR by controlling the timely recruitment of repair factors at DSBs, including RPA, RAD51, and 53BP1 (Alfano et al., 2019; Brustel et al., 2018; Burger et al., 2019; Cohen et al., 2018; D'Alessandro et al., 2018; Domingo-Prim et al., 2019; Li et al., 2016; Lu et al., 2018; Ohle et al., 2016; Yasuhara et al., 2018). At transcriptionally active loci, R-loops were shown to trigger an XPG-dependent non-canonical mechanism of DSB resection, favoring HDR over NHEJ

(Yasuhara et al., 2018). On the other hand, persistent DNA:RNA hybrids around broken ends interfere with the DSB repair fidelity, as observed in human cells lacking the helicase Senataxin (SETX), a central enzyme involved in DNA:RNA hybrid clearance (Brustel et al., 2018; Cohen et al., 2018). Hybrid accumulation due to the inactivation of the exosome catalytic subunit EXOSC10 (Domingo-Prim et al., 2019), or the RNA binding protein HNRNDP (Alfano et al., 2019), also impairs HDR by altering the speed of DSB resection. Overall, it seems that DNA:RNA hybrids generated by pre-existing transcription could block DSB processing and/or repair (Alfano et al., 2019; Cohen et al., 2018; Costantino and Koshland, 2018; Domingo-Prim et al., 2019), whereas hybrids resulting from DSB-induced transcription stimulate resection (Domingo-Prim et al., 2019) and repair (D'Alessandro et al., 2018; Ohle et al., 2016).

Overall, the mechanism(s) by which DNA:RNA hybrids influence DSB resection and DSB repair choice remain poorly understood (Jimeno et al., 2019; Marini et al., 2019).

To unravel the mechanism by which DNA:RNA hybrids interfere with the repair of DSBs, we utilized a model system in which an inducible HO endonuclease creates a single DSB at the *MAT* locus in budding yeast. This system has been broadly used to characterize DSB repair mechanisms in eukaryotes (Haber, 2012). Specifically, we studied yeast cells carrying mutations in Sen1, the ortholog of human Senataxin, whose dysfunctions are linked to neurological disorders and cancer (Groh et al., 2017). We found that DNA:RNA hybrids were accumulated at a single HO-induced DSB (HO-DSB) in cells lacking functional Sen1. This hybrid accumulation was associated with prolonged binding of KU at the break and increased mutagenic NHEJ events. Moreover, local DNA:RNA hybrids primed a non-canonical Mre11- and Dna2- dependent DSB resection initiation promoting HDR repair.

Our results demonstrate that accumulated DNA:RNA hybrids proximal to the break site affect DNA repair fidelity and appropriate processing of DSB, resulting in threats to genome stability.

RESULTS

Sen1 Helicase Limits DNA:RNA Hybrids at a DSB and Alters End Resection

We investigated the functional crosstalk between DSB repair and DNA:RNA hybrids, focusing our attention on the anti-R-loop Sen1 helicase in budding yeast. First, we analyzed the Sen1 enrichment at HO-DSB at *MATa* locus by chromatin immunoprecipitation (ChIP) (Figure 1A). Sen1 binding was tested in wild-type cells together with *sae2Δ* and *mre11Δ* mutants, which are defective in short-range DSB resection (Symington, 2016). Sen1 levels increased near the DSB in wild-type and in *sae2Δ* cells, but not in *mre11Δ* cells (Figure 1B). Thus, Sen1 is recruited at the break through Mre11, regardless of the initial resection of the DSB. The presence of Sen1 at the HO-DSB prompted us to test whether DNA:RNA hybrids were accumulated at the break using DNA:RNA immunoprecipitation (DRIP) with the S9.6 antibody. We found a slight but reproducible increase of DRIP signals at both sides of the HO-DSB in wild-type cells (Figures 1C and 1D). Hybrid levels further increased upon depletion of Sen1 protein (Figures 1C and 1D), by means of a tetracycline-

mediated translational inhibition system (Figures S1A–S1C; Kötter et al., 2009). The DRIP signals were almost completely reverted by *in vitro* treatment with RNase H1 (Figure S1D), which is known to degrade DNA:RNA hybrids.

Taken together, the above results indicate that Sen1 is recruited at an HO-DSB via Mre11 and limits the accumulation of DNA:RNA hybrids proximal to the break. Then, we asked whether increased DNA:RNA hybrids near the HO-DSB in cells lacking Sen1 may interfere with the end resection, leading to the formation of the 3′ ssDNA. Using a qPCR-based approach (Ferrari et al., 2018), we observed higher levels of ssDNA at left and right sides near the HO-cut in Sen1-depleted cells when compared with the wild-type strain (Figures 1E and 1F). Notably, the presence of DNA:RNA hybrids might interfere with the detection of the ssDNA in our resection assay. Indeed, hybrids are notoriously stable and could be maintained in genomic DNA preparations, thus interfering with the cleavage of the restriction enzyme used during the ssDNA analysis. To exclude this possibility, we treated the DNA preparations with RNase H1 *in vitro*, before the restriction digestion and qPCR analysis. As shown in Figure S1E, the ssDNA levels remained higher in Sen1-depleted cells despite the RNase H1 treatment, indicating that the DNA is effectively resected. We also observed a higher amount of ssDNA at the HO-cut both by qPCR and Southern blotting in *sen1*-1 cells (Figure S2), which carry the G1747D mutation in the essential helicase domain (DeMarini et al., 1992). Notably, at distal regions from the break, the levels of ssDNA by qPCR (Figures S2A–S2C) and Southern blotting (Figures S2D–S2G) appeared similar in wild-type and *sen1*-1 cells. Taken together, these data indicate that DSB resection is not only proficient in the absence of Sen1 protein, but also results in larger amounts of ssDNA near the break, implying increased resection. Notably, the overexpression of *RNH1* in Sen1-depleted cells reduced the amount of ssDNA at the HO-DSB when compared with wild type (Figure 1G). These results indicate that DNA:RNA hybrids formed near the HO-DSB alter end resection, leading to increased ssDNA in the absence of Sen1. This resection profile resembles hyper-resection induced by *de novo* transcription at the break in EXOSC10-depleted human cells (Domingo-Prim et al., 2019). Based on this similarity and our observation that the level of local DNA:RNA hybrids increased after the HO break (Figures 1C and 1D), we suggest that these hybrids could be more likely formed by *de novo* RNA synthesis rather than pre-existing transcription.

Likewise to Sen1 depletion, the inactivation of the RNase H1/H2 enzymes through the double deletion of the *RNH1* and *RNH201* genes severely affects the processing of DNA:RNA hybrids and genome stability (Cerritelli and Crouch, 2009; Lazzaro et al., 2012). In fission yeast, RNase H enzymes have been implicated in limiting DNA:RNA hybrid accumulation at DSBs (Ohle et al., 2016), although whether they are essential in DSB repair is debatable (Zhao et al., 2018). To investigate the RNase H1/H2 roles in our context, we tested DSB resection in the double-mutant *rnh1Δ rnh201Δ*. We found that the complete inactivation of RNase H activities did not alter the kinetics of DSB resection initiation (Figure S3), implying that Sen1, rather than RNase H, plays a critical role in removing hybrids at DSBs in budding yeast.
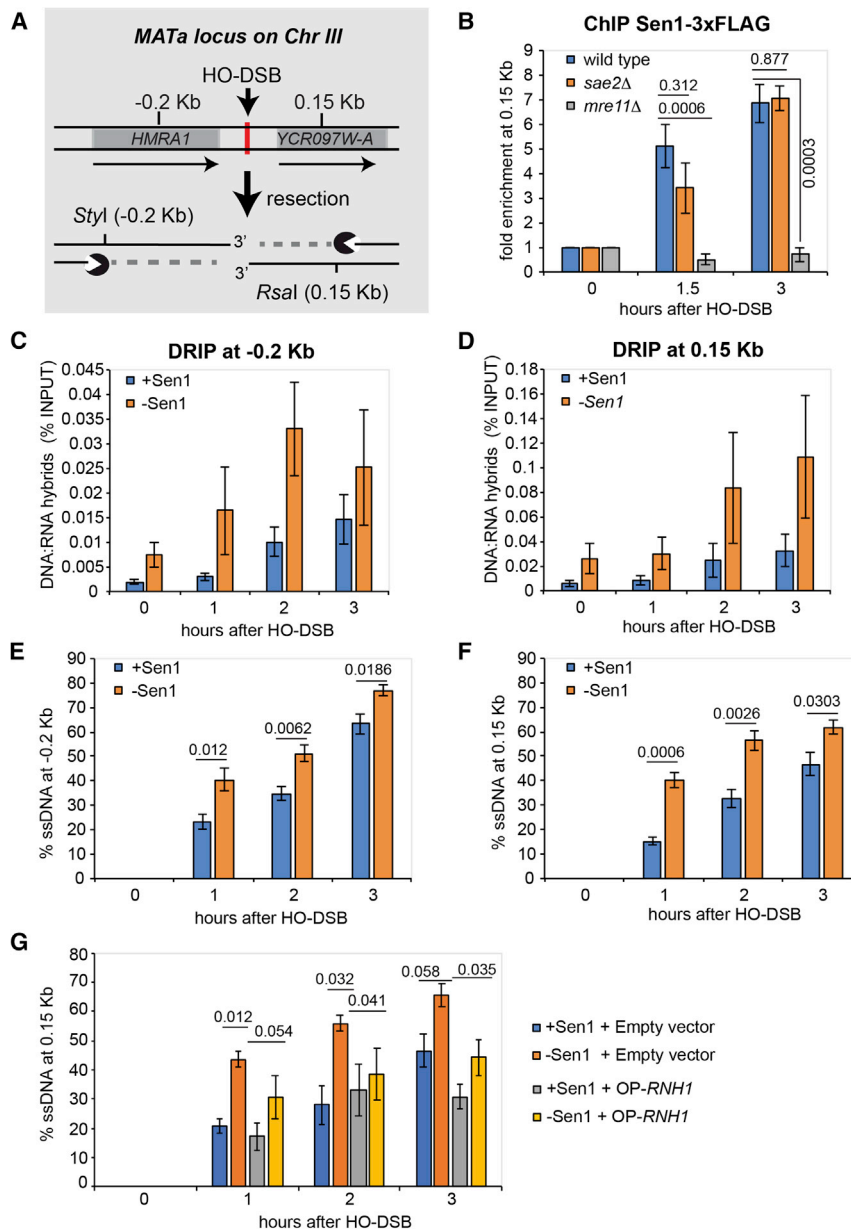
reduced in the absence of Sae2 (Figure S4A), which is required for the full activation of the Mre11 nuclease (Symington, 2016). Thus, Mre11 aided by Sae2 is necessary to initiate DSB resection also in Sen1-depleted cells. Accordingly, Mre11 is recruited at the HO-DSB in Sen1-depleted cells (Figure 2B). Moreover, we found that the binding levels of Mre11 were high without Sen1, resembling *sae2Δ* rather than the wild-type cells. Intriguingly, Mre11 binding decreased in Sen1-depleted cells at 3 h after the DSB (Figure 2B), implying functional resection (Figures 1E–1G). Overall, these data indicate that Mre11 is loaded at the DSB in the absence of Sen1. However, the Mre11 hyper-accumulation at the DSB suggests that the DNA:RNA hybrids are a physical hindrance for the Mre11 nuclease. In Sen1-depleted cells, Mre11 is also hyper-accumulated at *PDC1* (Figure S4B), a highly expressed gene prone to R-loop accumulation during the conflicts with the replication forks (Figure S4C; Brambati et al., 2018). However, contrary to its role in DSB resection initiation, Mre11 is known to play a structural role at sites of persistent R-loops rather than directly process them through its nuclease activity (Brambati et al., 2018; Chang et al., 2019).

Moreover, the higher levels of ssDNA at the HO-DSB found in *sen1* mutants were abrogated by auxin-dependent degradation

Mre11 and Dna2 Prime Non-canonical DSB Resection in the Absence of Sen1

The increased levels of ssDNA at the break in *sen1* mutants suggest that DSB resection is carried out faster and/or through a non-canonical mechanism facilitated by DNA:RNA hybrids. To delineate the nucleolytic pathway responsible for DSB resection initiation in the absence of functional Sen1, we performed qPCR assays in cells carrying mutations in *MRE11*, *SAE2*, *DNA2*, *SGS1*, and *EXO1*, which are involved in DSB resection.

It is known that DSB resection is severely compromised in the nuclease-defective *mre11*-H125D mutant (Moreau et al., 1999). As shown in Figure 2A, the amount of ssDNA detected by qPCR in *mre11*-H125D cells was severely reduced irrespective of Sen1 expression. The ssDNA levels were also partially

A

B ChIP Mre11-18Myc
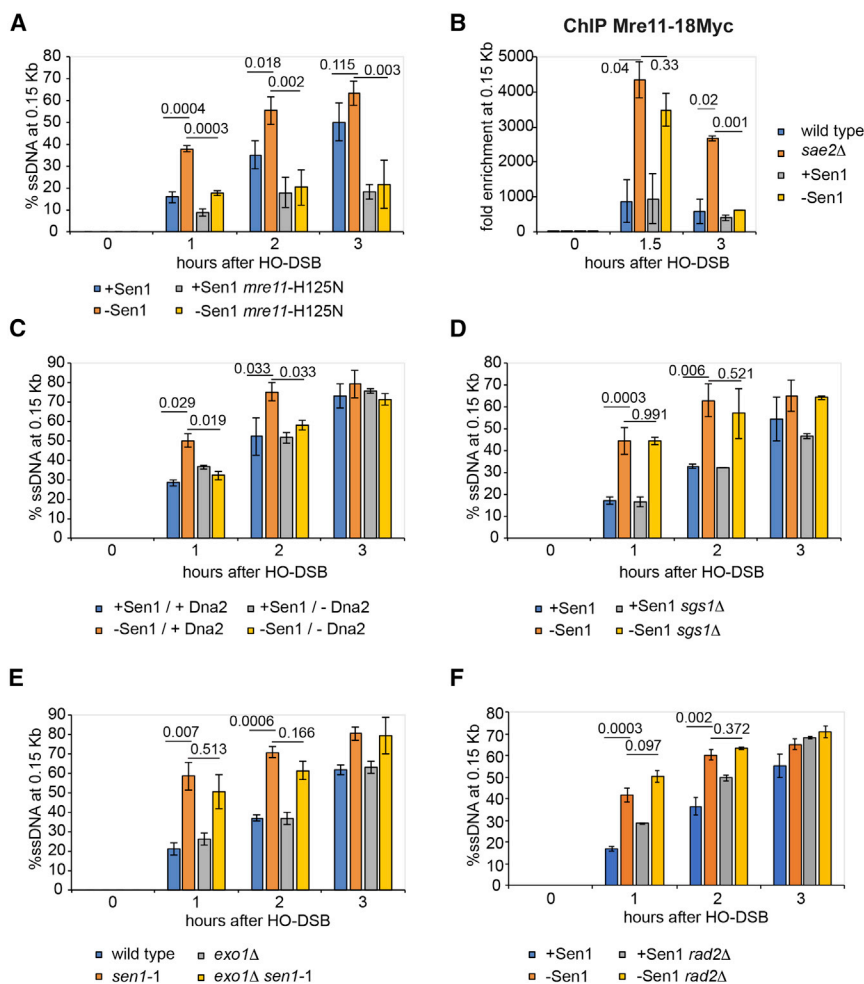
C

D

E

F

Figure 2. Mre11 and Dna2, but Not Sgs1 and Exo1, Initiate End Resection in the Absence of Sen1

(A) DSB resection analysis by qPCR in JKM139 derivative strains at 0.15 kb from DSB. Cells were blocked in G2/M phase by nocodazole, before *GAL::HO* induction. Translational inhibition of Sen1 in wild-type or *mre11*-H125N backgrounds was achieved by adding (−Sen1) or not (+Sen1) 500 μM tetracycline 4 h before DSB induction. Data represent mean ± SEM of at least three independent experiments. p values are indicated.

(B) Analysis of Mre11 binding by ChIP at 0.15 kb from DSB in JKM139 derivative strains. Cells were blocked in G2/M phase by nocodazole, before *GAL::HO* induction. Translational inhibition (−Sen1) or not (+Sen1) of Sen1 was achieved by adding 500 μM tetracycline 4 h before DSB induction. Data represent two independent experiments ± SEM. p values are indicated.

(C–F) DSB resection analysis by qPCR in JKM139 derivative strains at 0.15 kb from DSB to test the contribution of Dna2 (C), Sgs1 (D), Exo1 (E), and Rad2 (F). Data represent two independent experiments ± SEM. p values are indicated. Cells were blocked in G2/M phase by nocodazole, before *GAL::HO* induction. Translational inhibition of Sen1 and the degradation of Dna2 were achieved, respectively, by adding 500 μM tetracycline 4 h (−Sen1) and 1 mM auxin 1 h (−Dna2) before DSB induction.

See also Figure S4.

of Dna2 (Figure 2C; Ferrari et al., 2015), but not by the inactivation of Sgs1 or Exo1 (Figures 2D and 2E).

Taken together, the results in Figure 2 indicate that, when DNA:RNA hybrids persist near the break, Mre11 and Dna2 cooperate to prime a non-canonical DSB resection initiation that neither requires Sgs1 to unwind DNA nor Exo1 to degrade DNA ends.

The nucleotide excision repair XPG/Rad2 endonuclease is known to process R-loops (Cristini et al., 2019; Makharashvili et al., 2018; Sollier et al., 2014), also priming non-canonical DSB resection at transcribed regions (Yasuhara et al., 2018). However, we found that the deletion of *RAD2* did not contribute to the DSB resection initiation either per se or in combination with *sen1* mutant (Figure 2F), suggesting that, in our context, DNA:RNA hybrids trigger end processing via a different mechanism.

Sen1 Limits NHEJ and Translocations Events, but Not HDR

The accumulation of DNA:RNA hybrids at the HO-DSB and the non-canonical mechanism of end resection initiation in the absence of Sen1 prompted us to test the impact of Sen1 on

DSB repair. Southern blotting analysis of the HO-DSB at the *MAT* locus provided a quantitative measure of HDR and NHEJ repair (Figure 3A). In this assay, the DSB is repaired through gene conversion, leading to the replacement of *MAT*a by *MAT*alpha (Haber, 2012). NHEJ may also contribute to the repair, although at low frequency. As shown in Figures 3B and 3C, we found that HDR was functional in cells lacking Sen1 even though there was a slight reduction as compared with cells expressing Sen1. Thus, we conclude that the non-canonical mechanism to initiate resection in Sen1-depleted cells does not limit HDR repair of one HO-DSB. However, we also noted a significant increase in NHEJ repair products in Sen1-depleted cells as compared with wild-type cells (Figures 3B and 3C). Therefore, we decided to investigate the impact of the *sen1* mutation on NHEJ in more detail. We used a specific genetic system (Villarreal et al., 2012), in which HO cuts two different chromosomes, priming inter- and intra-chromosomal NHEJ repair, as well as inter-chromosomal MMEJ repair (trans/MMEJ) (Figure 3D). The different classes of events were determined by cell viability in selective media. We found increased rates of all of the repair events in *sen1*-1 cells compared with wild-type (Figure 3E). In conclusion, although HDR is mostly proficient in *sen1* mutants, the NHEJ and MMEJ events are increased.

We further investigated the contribution of Sen1 in mutagenic NHEJ using another repair assay. In this system, the frequency of
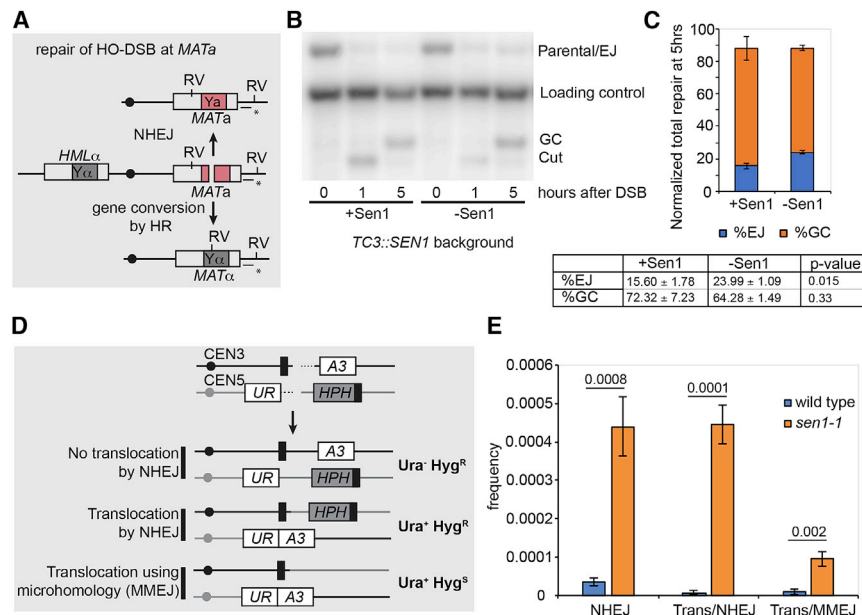
Figure 3. Sen1 Inactivation Does Not Impair *MAT* Switching but Increases NHEJ and Trans/MMEJ

(A) Experimental system to study gene conversion in JKM161. The location of *MAT*-specific probe (*) and the restriction endonuclease *Eco*RV (RV) cleavage sites used for Southern blot analysis are shown.

(B and C) Southern blot (B) and quantification analysis (C) of the DSB repair product formation by homologous recombination (HR) and NHEJ upon HO-induction in nocodazole-arrested cells. Data represent the mean ± SEM of three independent experiments.

(D) Experimental system to study HO-inducible inter- and intra-chromosomal NHEJ and inter-chromosomal MMEJ (trans/MMEJ) in YDV500.17 background.

(E) Frequencies of the repair outcomes in wild-type and *sen1*-1 in YDV500.17 derivative strains. The results are the average of three independent experiments ± SEM. p values are indicated.

EJ, end joining; GC, gene conversion.

cell survival is calculated after persistent DSB induction at the *MAT* locus, which results in HO recognition site corruption and re-ligation (Ma et al., 2003). We observed an ~5-fold increase in the frequency of imprecise NHEJ of one HO-DSB in *sen1*-1 cells compared with wild-type (Figure 4A). The imprecise NHEJ events observed in wild-type and in *sen1*-1 cells were completely abolished after the deletion of *KU70* (Figure 4A). Consistent with this, the binding of Ku70 at the DSB was higher in the absence of Sen1 (Figure 4B). We asked whether the increase in NHEJ events and KU binding in *sen1* mutants were dependent on DNA:RNA hybrid accumulation at the DSB. We found that *RNH1* overexpression prevented the increased binding of Ku70 in Sen1-depleted cells (Figure 4B) and partially limited the NHEJ events in *sen1*-1 cells (Figure 4C). Taken together, these findings indicate that DNA:RNA hybrid accumulation nearby a DSB triggers KU-dependent mutagenic NHEJ.

DISCUSSION

Transcription was shown to positively or negatively interfere with DSB repair (Jimeno et al., 2019; Marini et al., 2019; Puget et al., 2019). In particular, it is an open debate whether DNA:RNA hybrids and/or R-loops near a DSB might interfere with DNA end resection. To complicate the picture, recent findings suggest that, not only pre-existing transcription at DSB, but also *de novo* transcription initiation engaged at DSB ends can be a source of hybrids (Jimeno et al., 2019; Marini et al., 2019; Puget et al., 2019). Particularly, *de novo* transcription divergent from the DSB has been recently observed in different genomic contexts and by different approaches (D'Alessandro et al., 2018; Domingo-Prim et al., 2019; Michelini et al., 2017; Vitor et al., 2019).

Here we show that cells that lack functional Sen1 have elevated levels of DNA:RNA hybrids close to a DSB. Because hybrids increase after break formation and during resection, they are expected to engage the 3′ end of the non-resected strand (Figure 5), although they may form also on the other filament. Moreover, our data indicate that hybrids stimulate rather than prevent resection, suggesting that *de novo* DSB-induced transcription could contribute to their formation, as described in other contexts (Domingo-Prim et al., 2019). In the absence of Sen1, we indeed found that resection is primed through a non-canonical mechanism utilizing DNA:RNA hybrid, Mre11 and Dna2, without the cooperation of Sgs1 to unwind DNA (Figure 5). An Sgs1-independent role for Dna2 in resecting DNA was recently demonstrated in specific conditions at telomeres (Markiewicz-Potoczny et al., 2018) and by *in vitro* assay (Paudyal et al., 2017). We suggest that in *sen1* mutants, Mre11 nicks the DNA and Dna2 cuts the 5′ end flap, which has been displaced from the template strand by divergent transcription from the break (Figure 5). However, in *sen1* mutants, the persistence of DNA:RNA hybrids in the vicinity of the DSB might interfere with the Mre11 activity, as recently supported by *in vitro* assay (Chang et al., 2019), resulting in its hyper-accumulation at the lesion. The current model suggests that Mre11 is also required to remove KU from the break, limiting NHEJ (Marini et al., 2019). Remarkably, both the Ku70 binding and NHEJ are increased in Sen1-depleted cells, and both depend on persistent DNA:RNA hybrids. Thus, we propose that the persistent hybrids hinder Mre11 activity and the timely removal of KU from the break, leading to NHEJ and chromosome translocations (Figure 5). Notably, Mre11 physically interacts with Sen1 (Yüce and West, 2013), and here we show that it recruits Sen1 at the DSB, supporting the notion that Sen1 might favor Mre11 activity by locally dismantling the DNA:RNA hybrids. However, our data indicate that Mre11 ultimately succeeds in cutting DNA ends, even in the absence of Sen1. According to our model, once Mre11 has nicked the DNA and Dna2 has cut the 5′ flap, we assume that DNA:RNA hybrids are processed by other helicases/nucleases, because the HDR repair of single HO-induced DSB is mostly proficient in
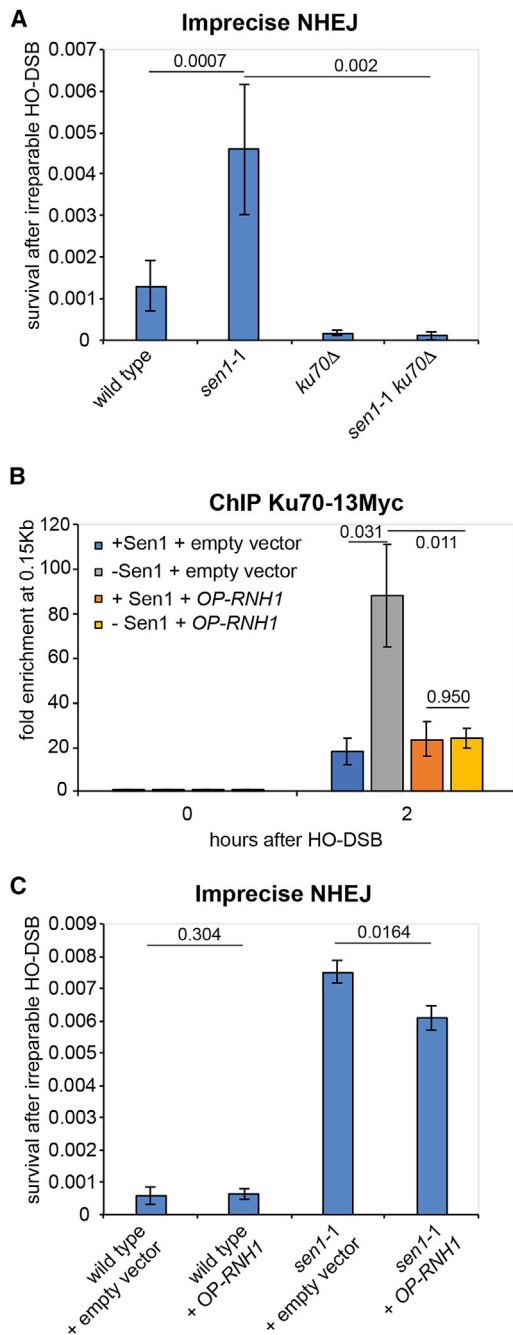
A

Imprecise NHEJ

B

ChIP Ku70-13Myc

C

Imprecise NHEJ

Figure 4. Prolonged Ku70 Binding and DNA:RNA Hybrids Increase Imprecise NHEJ in *sen1* Mutants

(A) Survival frequency of JKM139-derived strains after induction of single irreparable DSB. Data represent four independent experiments ± SEM. p values are indicated.

(B) Analysis of Ku70 binding by ChIP at 0.15 kb from the DSB. Cells over-expressing (*OP-RNH1*) or not (empty vector) *RNH1* were blocked in G2/M phase by nocodazole, before *GAL::HO* induction. The tetracycline addition leads to translation inhibition of Sen1 (−Sen1). Data represent four independent experiments ± SEM. p values are indicated.

(C) Survival frequency of JKM139-derived strains after induction of single irreparable DSB, with (*OP-RNH1*) or without (empty vector) the overexpression of *RNH1*. Data represent four independent experiments ± SEM. p values are indicated.
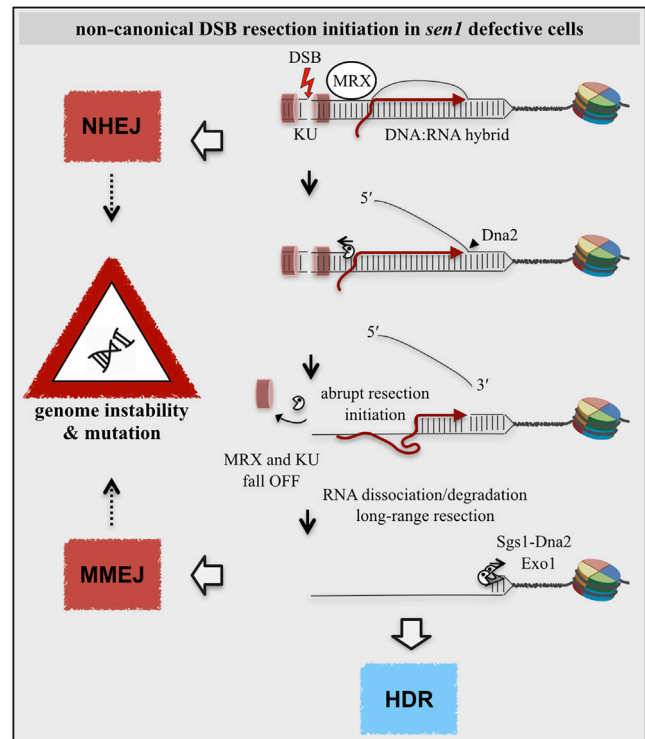

Figure 5. A Model for DSB Resection Initiation in the Context of DNA:RNA Hybrids without Functional Sen1

In the proximity of a DSB, local transcription from the DNA ends induces the formation of DNA:RNA hybrids, which, if not dissociated by Sen1, could interfere with the DSB resection process at different steps: (1) they hinder the DNA cutting activity of the Mre11 complex nearby the DSB, leading to a prolonged binding of the KU complex and increased non-homologous end joining (NHEJ) events; (2) after the Mre11 endo-nucleolytic cleavage of the 5′ strand, the DNA:RNA hybrids cause abrupt exposition of the 5′ ssDNA flap, which can be immediately cut by Dna2; and (3) when the 3′ filament is generated, the RNA is ultimately degraded or dissociated, promoting the repair through micro-homology-mediated end joining (MMEJ) or homology-directed recombination (HDR). See text for further details.

sen1 mutants. As such, the RNase H enzymes, whose inactivation is lethal in *sen1*-thermosensitive mutants (Appanah et al., 2020; Costantino and Koshland, 2018; Lockhart et al., 2019), could be involved. We found that the ablation of genes encoding RNase H1/2 did not alter per se DSB resection initiation. Nevertheless, we could not test whether RNase H enzymes play a role in DSB repair in the absence of Sen1, because their inactivation was lethal in our *sen1* conditional mutant strain.

We also suggest that the abrupt formation of ssDNA tract might contribute to the increase in MMEJ-mediated translocations found in *sen1*-1 cells (Figure 5). These findings are consistent with increased levels of spontaneous gene conversion and pop-out events in *sen1* mutants (Alzu et al., 2012; Mischo et al., 2011).

Although the non-canonical mechanism to prime DSB resection that we propose in our model is detrimental for genome integrity, leading to increased events of mutagenic NHEJ and chromosome translocations, it may work in certain pathological conditions, in which the canonical resection pathway is mutated.

Importantly, the Mre11- and Dna2-dependent DSB resection mechanism that we found here does not require XPG/Rad2 and is therefore distinct from the end processing described in human cells to initiate HDR at transcriptionally active loci (Yasuhara et al., 2018). Moreover, DNA endonucleases, including CtIP, cooperate to remove R-loops by dual incision (Cristini et al., 2019; Makharashvili et al., 2018; Sollier et al., 2014), raising the question whether the Mre11/Dna2-dependent pathway described here could be also implicated in dismantling persistent R-loops at DSBs and other genomic sites. We think this is unlikely, because other evidence indicates that Mre11 plays a nuclease-independent structural role at sites of persistent R-loops (Brambati et al., 2018; Chang et al., 2019).

Similar to our findings, elevated translocations and slight reduction of HDR due to hybrid accumulation at DSBs have been observed in human cells depleted for Senataxin (Cohen et al., 2018). However, contrary to our results, Senataxin depletion in human cells did not significantly affect resection (Cohen et al., 2018). However, we note that a link between hyper-resection and DNA:RNA hybrid accumulation near DSBs has been observed in human cells depleted of EXOSC10 (Domingo-Prim et al., 2019), and the RNA exosome complex physically and functionally interacts with Senataxin at DNA lesions (Richard et al., 2013).

Further investigations will be needed to verify whether the DSB resection mechanism that we described in yeast is conserved in human cells, which could be relevant for the comprehension of the molecular defects of genome instability syndromes associated with cancer and neurodegeneration.

STAR★METHODS

Detailed methods are provided in the online version of this paper and include the following:

- KEY RESOURCES TABLE
- LEAD CONTACT AND MATERIALS AVAILABILITY
- EXPERIMENTAL MODEL AND SUBJECT DETAILS
- METHOD DETAILS
  - Construction of yeast strains
  - Measurement of DSB resection at MAT locus
  - SDS-PAGE and western blot
  - Chromatin Immunoprecipitation (ChIP)
  - DNA:RNA immunoprecipitation (DRIP) analysis
  - MAT switching analysis by Southern blot
  - Imprecise NHEJ assay
  - Micro-homology mediated DSB repair assay
  - Quantification and statistical analysis
- DATA AND CODE AVAILABILITY

SUPPLEMENTAL INFORMATION

Supplemental Information can be found online at https://doi.org/10.1016/j.celrep.2020.107603.

AUTHOR CONTRIBUTIONS

Conceptualization, C.C.R., G.L., and A.P.; Investigation, C.C.R., L.Z., M.D.T., E.G., A.B., and F.L.; Writing – Original Draft, C.C.R., G.L., and A.P.; Writing – Review and Editing, C.C.R., G.L., and A.P.; Funding Acquisition, G.L. and A.P.; Supervision, G.L. and A.P.

DECLARATION OF INTERESTS

The authors declare no competing interests.

REFERENCES

Alfano, L., Caporaso, A., Altieri, A., Dell'Aquila, M., Landi, C., Bini, L., Pentimalli, F., and Giordano, A. (2019). Depletion of the RNA binding protein HNRNPD impairs homologous recombination by inhibiting DNA-end resection and inducing R-loop accumulation. Nucleic Acids Res. 47, 4068–4085.

Alzu, A., Bermejo, R., Begnis, M., Lucca, C., Piccini, D., Carotenuto, W., Saponaro, M., Brambati, A., Cocito, A., Foiani, M., and Liberi, G. (2012). Senataxin associates with replication forks to protect fork integrity across RNA-polymerase-II-transcribed genes. Cell 151, 835–846.

Appanah, R., Lones, E.C., Aiello, U., Libri, D., and De Piccoli, G. (2020). Sen1 Is Recruited to Replication Forks via Ctf4 and Mrc1 and Promotes Genome Stability. Cell Rep. 30, 2094–2105.e9.

Brambati, A., Zardoni, L., Achar, Y.J., Piccini, D., Galanti, L., Colosio, A., Foiani, M., and Liberi, G. (2018). Dormant origins and fork protection mechanisms rescue sister forks arrested by transcription. Nucleic Acids Res. 46, 1227–1239.

Brustel, J., Kozik, Z., Gromak, N., Savic, V., and Sweet, S.M.M. (2018). Large XPF-dependent deletions following misrepair of a DNA double strand break are prevented by the RNA:DNA helicase Senataxin. Sci. Rep. 8, 3850.

Burger, K., Schlackow, M., and Gullerova, M. (2019). Tyrosine kinase c-Abl couples RNA polymerase II transcription to DNA double-strand breaks. Nucleic Acids Res. 47, 3467–3484.

Castellano-Pozo, M., Santos-Pereira, J.M., Rondón, A.G., Barroso, S., Andújar, E., Pérez-Alegre, M., García-Muse, T., and Aguilera, A. (2013). R loops are linked to histone H3 S10 phosphorylation and chromatin condensation. Mol. Cell 52, 583–590.

Cerritelli, S.M., and Crouch, R.J. (2009). Ribonuclease H: the enzymes in eukaryotes. FEBS J. 276, 1494–1505.

Chang, E.Y., Tsai, S., Aristizabal, M.J., Wells, J.P., Coulombe, Y., Busatto, F.F., Chan, Y.A., Kumar, A., Dan Zhu, Y., Wang, A.Y., et al. (2019). MRE11-RAD50-NBS1 promotes Fanconi Anemia R-loop suppression at transcription-replication conflicts. Nat. Commun. 10, 4265.

Cohen, S., Puget, N., Lin, Y.L., Clouaire, T., Aguirrebengoa, M., Rocher, V., Pasero, P., Canitrot, Y., and Legube, G. (2018). Senataxin resolves RNA:DNA hybrids forming at DNA double-strand breaks to prevent translocations. Nat. Commun. 9, 533.

Costantino, L., and Koshland, D. (2018). Genome-wide Map of R-Loop-Induced Damage Reveals How a Subset of R-Loops Contributes to Genomic Instability. Mol. Cell 71, 487–497.e3.

Cristini, A., Ricci, G., Britton, S., Salimbeni, S., Huang, S.N., Marinello, J., Calsou, P., Pommier, Y., Favre, G., Capranico, G., et al. (2019). Dual Processing of R-Loops and Topoisomerase I Induces Transcription-Dependent DNA Double-Strand Breaks. Cell Rep. 28, 3167–3181.e6.

D'Alessandro, G., Whelan, D.R., Howard, S.M., Vitelli, V., Renaudin, X., Adamowicz, M., Iannelli, F., Jones-Weinert, C.W., Lee, M., Matti, V., et al. (2018). BRCA2 controls DNA:RNA hybrid level at DSBs by mediating RNase H2 recruitment. Nat. Commun. 9, 5376.

DeMarini, D.J., Winey, M., Ursic, D., Webb, F., and Culbertson, M.R. (1992). SEN1, a positive effector of tRNA-splicing endonuclease in Saccharomyces cerevisiae. Mol. Cell. Biol. 12, 2154–2164.

Domingo-Prim, J., Endara-Coll, M., Bonath, F., Jimeno, S., Prados-Carvajal, R., Friedländer, M.R., Huertas, P., and Visa, N. (2019). EXOSC10 is required for RPA assembly and controlled DNA end resection at DNA double-strand breaks. Nat. Commun. 10, 2135.

Ferrari, M., Dibitetto, D., De Gregorio, G., Eapen, V.V., Rawal, C.C., Lazzaro, F., Tsabar, M., Marini, F., Haber, J.E., and Pellicioli, A. (2015). Functional interplay between the 53BP1-ortholog Rad9 and the Mre11 complex regulates resection, end-tethering and repair of a double-strand break. PLoS Genet. 11, e1004928.

Ferrari, M., Twayana, S., Marini, F., and Pellicioli, A. (2018). A qPCR-Based Protocol to Quantify DSB Resection. Methods Mol. Biol. 1672, 119–129.

Foiani, M., Liberi, G., Lucchini, G., and Plevani, P. (1995). Cell cycle-dependent phosphorylation and dephosphorylation of the yeast DNA polymerase alpha-primase B subunit. Mol. Cell. Biol. 15, 883–891.

Frit, P., Ropars, V., Modesti, M., Charbonnier, J.B., and Calsou, P. (2019). Plugged into the Ku-DNA hub: The NHEJ network. Prog. Biophys. Mol. Biol. 147, 62–76.

Goldstein, A.L., and McCusker, J.H. (1999). Three new dominant drug resistance cassettes for gene disruption in Saccharomyces cerevisiae. Yeast 15, 1541–1553.

Groh, M., Albulescu, L.O., Cristini, A., and Gromak, N. (2017). Senataxin: Genome Guardian at the Interface of Transcription and Neurodegeneration. J. Mol. Biol. 429, 3181–3195.

Haber, J.E. (2012). Mating-type genes and MAT switching in Saccharomyces cerevisiae. Genetics 191, 33–64.

Jimeno, S., Prados-Carvajal, R., and Huertas, P. (2019). The role of RNA and RNA-related proteins in the regulation of DNA double strand break repair pathway choice. DNA Repair (Amst.) 81, 102662.

Kötter, P., Weigand, J.E., Meyer, B., Entian, K.D., and Suess, B. (2009). A fast and efficient translational control system for conditional expression of yeast genes. Nucleic Acids Res. 37, e120.

Lazzaro, F., Novarina, D., Amara, F., Watt, D.L., Stone, J.E., Costanzo, V., Burgers, P.M., Kunkel, T.A., Plevani, P., and Muzi-Falconi, M. (2012). RNase H and postreplication repair protect cells from ribonucleotides incorporated in DNA. Mol. Cell 45, 99–110.

Lee, S.E., Moore, J.K., Holmes, A., Umezu, K., Kolodner, R.D., and Haber, J.E. (1998). Saccharomyces Ku70, mre11/rad50 and RPA Proteins Regulate Adaptation to G2/M Arrest After DNA Damage. Cell 94, 399–409.

Li, L., Germain, D.R., Poon, H.Y., Hildebrandt, M.R., Monckton, E.A., McDonald, D., Hendzel, M.J., and Godbout, R. (2016). DEAD Box 1 Facilitates Removal of RNA and Homologous Recombination at DNA Double-Strand Breaks. Mol. Cell. Biol. 36, 2794–2810.

Lockhart, A., Pires, V.B., Bento, F., Kellner, V., Luke-Glaser, S., Yakoub, G., Ulrich, H.D., and Luke, B. (2019).). RNase H1 and H2 Are Differentially Regulated to Process RNA-DNA Hybrids. Cell Rep. 29, 2890–2900.e5.

Longtine, M.S., McKenzie, A., 3rd, Demarini, D.J., Shah, N.G., Wach, A., Brachat, A., Philippsen, P., and Pringle, J.R. (1998). Additional modules for versatile and economical PCR-based gene deletion and modification in Saccharomyces cerevisiae. Yeast 14, 953–961.

Lu, W.T., Hawley, B.R., Skalka, G.L., Baldock, R.A., Smith, E.M., Bader, A.S., Malewicz, M., Watts, F.Z., Wilczynska, A., and Bushell, M. (2018). Drosha drives the formation of DNA:RNA hybrids around DNA break sites to facilitate DNA repair. Nat. Commun. 9, 532.

Ma, J.L., Kim, E.M., Haber, J.E., and Lee, S.E. (2003). Yeast Mre11 and Rad1 proteins define a Ku-independent mechanism to repair double-strand breaks lacking overlapping end sequences. Mol. Cell. Biol. 23, 8820–8828.

Makharashvili, N., Arora, S., Yin, Y., Fu, Q., Wen, X., Lee, J.H., Kao, C.H., Leung, J.W., Miller, K.M., and Paull, T.T. (2018). Sae2/CtIP prevents R-loop accumulation in eukaryotic cells. eLife 7, e42733.

Marini, F., Rawal, C.C., Liberi, G., and Pellicioli, A. (2019). Regulation of DNA Double Strand Breaks Processing: Focus on Barriers. Front. Mol. Biosci. 6, 55.

Markiewicz-Potoczny, M., Lisby, M., and Lydall, D. (2018). A Critical Role for Dna2 at Unwound Telomeres. Genetics 209, 129–141.

Michelini, F., Pitchiaya, S., Vitelli, V., Sharma, S., Gioia, U., Pessina, F., Cabrini, M., Wang, Y., Capozzo, I., Iannelli, F., et al. (2017). Damage-induced lncRNAs control the DNA damage response through interaction with DDRNAs at individual double-strand breaks. Nat. Cell Biol. 19, 1400–1411.

Mischo, H.E., Gómez-González, B., Grzechnik, P., Rondón, A.G., Wei, W., Steinmetz, L., Aguilera, A., and Proudfoot, N.J. (2011). Yeast Sen1 helicase protects the genome from transcription-associated instability. Mol. Cell 41, 21–32.

Moreau, S., Ferguson, J.R., and Symington, L.S. (1999). The nuclease activity of Mre11 is required for meiosis but not for mating type switching, end joining, or telomere maintenance. Mol. Cell. Biol. 19, 556–566.

Ohle, C., Tesorero, R., Schermann, G., Dobrev, N., Sinning, I., and Fischer, T. (2016). Transient RNA-DNA Hybrids Are Required for Efficient Double-Strand Break Repair. Cell 167, 1001–1013.e7.

Paudyal, S.C., Li, S., Yan, H., Hunter, T., and You, Z. (2017). Dna2 initiates resection at clean DNA double-strand breaks. Nucleic Acids Res. 45, 11766–11781.

Puget, N., Miller, K.M., and Legube, G. (2019). Non-canonical DNA/RNA structures during Transcription-Coupled Double-Strand Break Repair: Roadblocks or Bona fide repair intermediates? DNA Repair (Amst.) 81, 102661.

Richard, P., Feng, S., and Manley, J.L. (2013). A SUMO-dependent interaction between Senataxin and the exosome, disrupted in the neurodegenerative disease AOA2, targets the exosome to sites of transcription-induced DNA damage. Genes Dev. 27, 2227–2232.

Seol, J.H., Shim, E.Y., and Lee, S.E. (2018). Microhomology-mediated end joining: Good, bad and ugly. Mutat. Res. 809, 81–87.

Sollier, J., Stork, C.T., García-Rubio, M.L., Paulsen, R.D., Aguilera, A., and Cimprich, K.A. (2014). Transcription-coupled nucleotide excision repair factors promote R-loop-induced genome instability. Mol. Cell 56, 777–785.

Symington, L.S. (2016). Mechanism and regulation of DNA end resection in eukaryotes. Crit. Rev. Biochem. Mol. Biol. 51, 195–212.

Villarreal, D.D., Lee, K., Deem, A., Shim, E.Y., Malkova, A., and Lee, S.E. (2012). Microhomology directs diverse DNA break repair pathways and chromosomal translocations. PLoS Genet. 8, e1003026.

Vitor, A.C., Sridhara, S.C., Sabino, J.C., Afonso, A.I., Grosso, A.R., Martin, R.M., and de Almeida, S.F. (2019). Single-molecule imaging of transcription at damaged chromatin. Sci. Adv. 5, eaau1249.

Yasuhara, T., Kato, R., Hagiwara, Y., Shiotani, B., Yamauchi, M., Nakada, S., Shibata, A., and Miyagawa, K. (2018). Human Rad52 Promotes XPG-Mediated R-loop Processing to Initiate Transcription-Associated Homologous Recombination Repair. Cell 175, 558–570.e11.

Yüce, Ö., and West, S.C. (2013). Senataxin, defective in the neurodegenerative disorder ataxia with oculomotor apraxia 2, lies at the interface of transcription and the DNA damage response. Mol. Cell. Biol. 33, 406–417.

Zhao, H., Zhu, M., Limbo, O., and Russell, P. (2018). RNase H eliminates R-loops that disrupt DNA replication but is nonessential for efficient DSB repair. EMBO Rep. 19, e45335.

Cell Reports
Article

STAR★METHODS

KEY RESOURCES TABLE

REAGENT or RESOURCE	SOURCE	IDENTIFIER
Antibodies		
Anti-FLAG M2 Magnetic beads	Sigma-Aldrich	M8823; RRID: AB_2637089
Anti-FLAG M2 antibody	Sigma-Aldrich	F1804; RRID: AB_262044
Anti-HA (12CA5)	autoproduction	N/A
Anti-Myc (9E10)	autoproduction	N/A
HRP conjugated goat anti-mouse antibody	Life Technologies	ab31430; RRID: AB_2040944
Anti-DNA:RNA hybrids S9.6	Marco Foiani Lab	N/A
Anti-PGK1 antibody	SantaCruz	sc-130335; RRID: AB_2268001
Bacterial and Virus Strains		
DH5alpha competent cells	Thermo Fisher Scientific	18265017
KAN::pADH1:TC3::3HA	Euroscarf	Lab stock B294
	Kötter et al., 2009	
	P30598	
pFA6a-KANMX6	Longtine et al., 1998	Lab stock B39
pFA6a-13Myc-KANMX6	Longtine et al., 1998	Lab stock B45
pFA6a-3HA-KANMX6	Longtine et al., 1998	Lab stock B70
pFA6a-TRP1MX6	Longtine et al., 1998	Lab stock B40
pAG25-NATMX4	Goldstein and McCusker, 1999	Lab stock B28
pAG32-HPHMX4	Goldstein and McCusker, 1999	Lab stock B29
pRS416-URA3	Federico Lazzaro lab	Lab stock B303
pFA6a-2xFLAG-KANMX6	Federico Lazzaro lab	Lab stock B284
ptetO7::RNH1	Andres Aguilera lab	Lab stock B419
Chemicals, Peptides, and Recombinant Proteins		
Tetracycline hydrochloride	Sigma-Aldrich	T7660-25G
Nocodazole	USBiological	N3000
Dynabeads Protein G	Thermo Fischer Scientific	10004D
Dynabeads Protein A	Thermo Fischer Scientific	10002D
RNase H	NEB	M0297S
*Rsa*I	NEB	R0167S
*Sty*I-HF	NEB	R3500S
*EcoR*V-HF	NEB	R3195S
PerfectHyb Plus Hybridization Buffer	Sigma-Aldrich	H7033-1L
Realtime PCR 2xMastermix	Genespin srl	QSTS-SMMix500
QIAGEN QuantiFast SYBR Green PCR Kit	QIAGEN	204056
ddPCR supermix evagreen	Biorad	1864033
Hygromycin B	Merck-Millipore	400050-5GM
ClonNAT (nourseothricin)	Werner Bioagents	CAS#96736-11-7
cOmplete ULTRA Tablets, Mini, Protease Inhibitor Cocktail	Roche	5892970001
Proteinase K	Amsbio	120493-1
RNase A	Sigma-Aldrich	R6513
Critical Commercial Assays		
Wizard SV Gel and PCR Clean-Up System	Promega	A9282
DECA-prime II Random Primed DNA labeling Kit	Ambion- Thermo Fischer Scientific	AM1455
QIAGEN QIAquick PCR Purification kit	QIAGEN	28106

(Continued on next page)

Continued

REAGENT or RESOURCE	SOURCE	IDENTIFIER
NuPAGE 3-8% Tris-Acetate Gel 1.0mmX10 well	Thermo Fischer Scientific	EA0375BOX
Clarity Western ECL Substrate	Biorad	1705061
Droplet generation oil	Biorad	1864005
Droplet generator gasket	Biorad	1863009
Droplet Generator cartridge	Biorad	1864008
Experimental Model: *S. cerevisiae*		
List of strains used in the study:	Table S1	N/A
Oligonucleotides		
List of oligonucleotides used in the study:	Table S2	N/A
Software and Algorithms		
ImageJ	NIH	https://imagej.nih.gov/ij
Image Lab	Bio-Rad	https://www.bio-rad.com
Typhoon FLA 7000 control software	GE Healthcare	https://www.gelifesciences.com/en/us
Image-Quant	GE Healthcare	https://www.gelifesciences.com/en/us
Graph-pad Prism 6	Graphpad.com	https://www.graphpad.com/
Other:		
Typhoon- FLA 7000	GE Healthcare	https://www.gelifesciences.com/en/us
Biorad CFX Connect	Bio-Rad	https://www.bio-rad.com
Biorad Droplet Digital PCR	Bio-Rad	https://www.bio-rad.com
Roche Light Cycler 480 Real-Time PCR System	Roche	https://lifescience.roche.com/en_us.html

LEAD CONTACT AND MATERIALS AVAILABILITY

Further information and request for resources and reagents should be directed and will be fulfilled by the Lead Contact, Dr. Achille Pellicioli (achille.pellicioli@unimi.it).

The unique reagents and strains generated in this study are available from the Lead Contact upon request.

EXPERIMENTAL MODEL AND SUBJECT DETAILS

Saccharomyces cerevisiae is the experimental model used in this study. All strains are derivatives of *JKM139*, *JKM161, W303* and *YDV500.17* and are listed in Table S1. If not otherwise specified, cells were grown in YEP medium enriched with 2% glucose (YEP+glu), 3% raffinose (YEP+raf) or 3% raffinose and 2% galactose (YEP+raf+gal). All the experiments for *sen1*-1 were performed growing the cells overnight at 25°C and shifting to 33°C (semi-permissive temperature) half an hour before DSB induction. All the experiments using *TC3::SEN1* system were done at 28°C. Experiments with RNH1 overexpression (*OP-RNH1*) were done by pre-inoculating the cells in Synthetic Complete medium without Uracile (SC-Ura) enriched with 2% glucose, then shifting the cell culture overnight in YEP+raf. Further specifications are mentioned in the Method Details sections.

METHOD DETAILS

Construction of yeast strains

Deletions and tag fusions were generated by the one-step PCR method (Longtine et al., 1998). *sen1*-1 mutation was integrated by one-step PCR and confirmed by sequencing. Tetracycline mediated translational inhibition system for Sen1 (*pADH1-TC3::3HA-SEN1* or briefly *TC3::SEN1*) was created by one-step PCR for promoter replacement using p30598 as template (Kötter et al., 2009). Integration was confirmed by PCR and monitored by drop test on YEP+glu plates containing tetracycline 500 μM. Translational inhibition was confirmed by western blot analysis using anti-HA antibody. According to Ferrari et al. (2015), the degradation of the Dna2-DEG variant was induced by the addition of 1mM auxin in the medium. Plasmid *ptetO7::RNH1* for the overexpression of *RNH1* has been previously described (Castellano-Pozo et al., 2013).

Measurement of DSB resection at MAT locus

JKM139 derivative strains were grown to log phase in YEP+raf and arrested in G2/M with 20 μg/mL nocadozole and with or without tetracycline (500 μM) for 4 hours before addition of galactose to a final concentration of 2%. DSB end resection was analyzed by alkaline agarose gels using a single-stranded RNA probe as described previously (Ferrari et al., 2015) and by quantitative PCR

(qPCR) analysis (Ferrari et al., 2018). The oligonucleotides used in qPCR analysis are listed in Table S2. The DNA was digested with the *Rsa*I at 0.15 kb, 4.8 kb and 10 kb from the HO-cut site, or with *Sty*I at −0.2 kb from the HO-cut site. The *PRE1* and *KCC4* loci were used as controls. To rule out the inefficient digestion of DNA due to persistent DNA:RNA hybrids and consequent PCR amplification, the extracted genomic DNA was treated overnight with RNase H (NEB) and then was digested with *Rsa*I (Figure S1E).

SDS-PAGE and western blot

TCA protein extracts were prepared as described previously (Foiani et al., 1995) and separated by 3%–8% Tris acetate gradient gels (Invitrogen) for 3xHA-Sen1 analyses. Western blotting was performed using anti-HA (12CA5), anti-MYC (9E10), anti- FLAG (clone M2, Sigma-Aldrich) and anti-PGK1 (AbCam) antibodies.

Chromatin Immunoprecipitation (ChIP)

Cells were grown to log phase in YEP+raf and arrested in G2/M with 20 μg/mL nocodazole with or without tetracycline (500 μM) before addition of galactose to a final concentration of 2%. Cells were sampled before addition of galactose (0hr) and at time points after DSB induction as shown in respective figures. Samples were processed as previously described (Ferrari et al., 2015). Cells were crosslinked with 1% formaldehyde for 15 min for Sen1-3xFLAG, 5 min each for Mre11-18xMyc and Ku70-13Myc tagged proteins. The reaction was stopped by adding 0.125M Glycine for 5 min. Immunoprecipitation was performed by incubating the samples with Dynabeads Protein G (Thermo Fisher Scientific), previously conjugated with antibodies (15 μL Dynabeads pre-conjugated with anti-FLAG M2 antibody for Sen1-3xFLAG and 5 μg of 9E10 anti-Myc antibody for Mre11-18xMyc and Ku70-13xMyc) for 2 hours at 4°C. qPCR was done using oligonucleotides listed in Table S2. Data are presented as fold enrichment at the HO cut site (0.15 kb from DSB) over that at the *PRE1* locus on chromosome V and normalized to the corresponding input sample. All the ChIP experiments were performed at 28°C.

For ChIP of Mre11-FLAG at highly transcribed region (*PDC1*) (Figure S4B), cells were grown to log phase in YEP+gal and arrested in G1 with 2 μg/mL alpha-factor in YEP+glu to depleted Sen1 protein (Alzu et al., 2012). Cells were released in S-phase in the presence of 0.2M HU. Samples were crosslinked with 1% formaldehyde for 15 min. Purified crosslinked chromatin was sheared to 500-1000 bp by sonication and incubated overnight with 5 μL of anti-FLAG (ANTI-FLAG M2) monoclonal antibody bound to Dynabeads protein G beads. For each sample 5 μL was taken as INPUT. Input and immunoprecipitated samples were treated with protease K and RNase A before being isolated with the QIAquick PCR Purification Kit and then subjected to qPCR using the SYBR Green (QIAGEN QuantiFast SYBR Green). Samples were run in Roche Light Cycler 480 Real-Time PCR System. DNA enrichment was determined by quantitative PCR (qPCR) as follows: $100 \times 2^{\wedge}$ (CT adjusted INPUT – CT IP anti-FLAG). Each reaction was performed in triplicate. The standard deviations are calculated on the basis of at least three independent experiments.

DNA:RNA immunoprecipitation (DRIP) analysis

DNA:RNA hybrids were extracted and analyzed by immunoprecipitation using S9.6 antibodies followed by qPCR analysis, as previously described (Alzu et al., 2012). The treatment with RNase H (New England Biolabs) was performed overnight at 37°C on the genomic material before S9.6-immunoprecipitation (Figure S1D). Enrichment of DNA:RNA hybrids by qPCR was determined as follows: $100 \times 2^{\wedge}$ (CT adjusted INPUT – CT IP S9.6). Each reaction was performed in triplicate. The standard deviations are calculated on the basis of at least three independent experiments.

MAT switching analysis by Southern blot

Physical analysis of DSB repair during *MAT* switching in *JKM161* strain (Lee et al., 1998) was performed with DNA samples isolated at indicated time points in Figures 3A–3C. *HO* expression was suppressed by addition of 2% glucose 1hr after galactose addition. Genomic DNA was digested with *EcoR*V enzyme and separated on a 1% agarose gel. Southern blotting was done using a 1000 bp *MAT* probe. Loading was normalized to unprocessed *HIS3* gene. Densitometric quantification of the band intensity was performed using the ImageJ software. The SEM was calculated on three independent experiments.

Imprecise NHEJ assay

Survival after DSB through imprecise NHEJ in *JKM139* derivative strains was done by growing the cells overnight at 25°C in YEP+raf and shifting to the semi-permissive temperature of 33°C for sen1-1 mutant half an hour before plating. 25 μL of 1x106 cells/ml of each strain was plated on YEP+gal plates and a suitable dilution was plated on YEP+glu plates to measure viable cell count of the culture. Plates were incubated at 25°C for 3-4 days. The survival frequency was calculated by dividing the number of colonies obtained on YEP+gal plates by total number of cells plated. For strains harboring the empty vector or the RNH1 overexpressing plasmid (*OP-RNH1*), the assay was done by pre-inoculating the cells in glucose containing SC-Ura medium, then shifting the cell cultures overnight in YEP+raf. SEM was calculated on three or more independent experiments.

Micro-homology mediated DSB repair assay

YDV500.17 derivative strains (Villarreal et al., 2012) were grown overnight at 25°C in YEP+raf and shifted to the semi-permissive temperature of 33°C for *sen1*-1 mutant half an hour before plating. 100 μL of 1x10^7 cells/ml of each strain was plated in YEP+gal plates and a suitable dilution was plated in YEP+glu plates to measure viable cell count of the culture. Plates were incubated at 25°C for

3-4 days. The survival frequency was calculated by dividing the number of colonies obtained on YEP+gal plates by total number of cells plated. The YEP+gal plates were replicated on YEP+glu containing hygromycin (HPH) and glucose containing SC-Ura plates to screen for the type of events. SEM was calculated on three independent experiments.

Quantification and statistical analysis

Data are expressed as ± standard error of the mean (SEM) unless otherwise stated. Statistical tests were performed using the Student's t test using Graph-pad Prism 6. p values were determined by an unpaired two-tailed t test. No statistical methods or criteria were used to estimate sample size or to include or exclude samples.

DATA AND CODE AVAILABILITY

This study did not generate/analyze datasets/code.